Utilizing the cold sintering process for sintering the thermally decomposable lead dioxide

I. A. D. Al-Hydary, A. M. Abdullah & M. A. A. Al-dujaili

Journal of the Australian Ceramic Society

ISSN 2510-1560

J Aust Ceram Soc
DOI 10.1007/s41779-019-00432-5

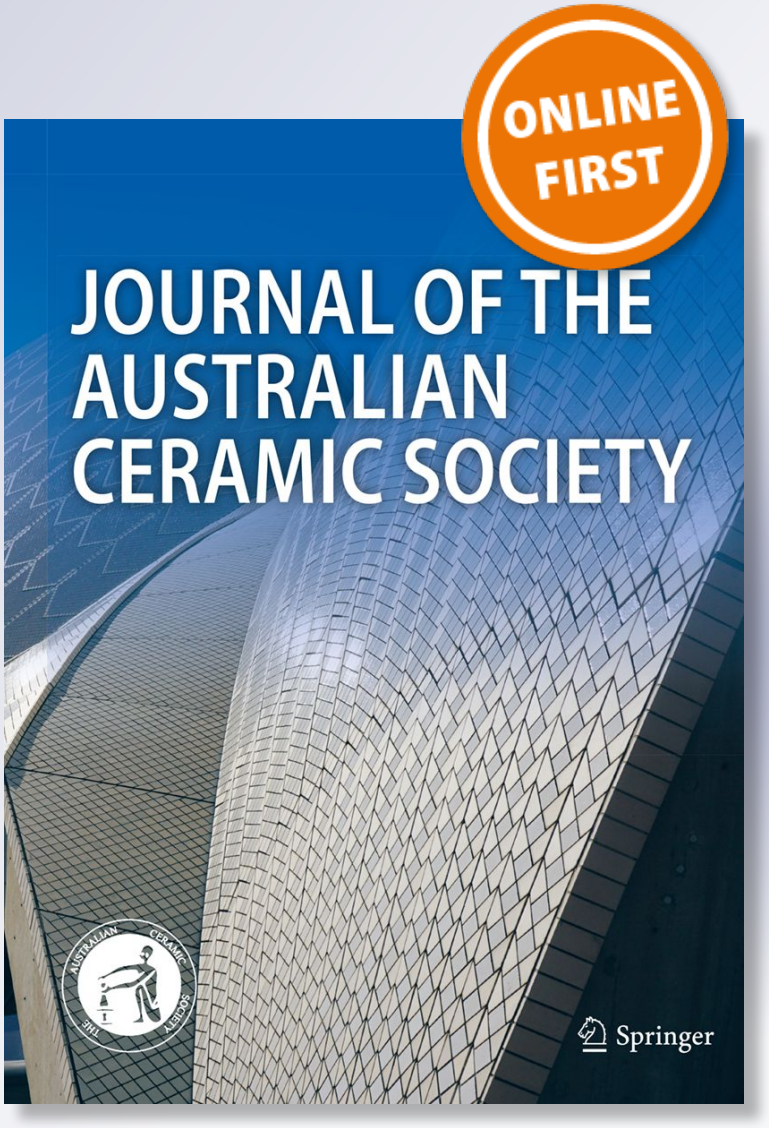

Springer

Journal of the Australian Ceramic Society
https://doi.org/10.1007/s41779-019-00432-5

RESEARCH

Utilizing the cold sintering process for sintering the thermally decomposable lead dioxide

I. A. D. Al-Hydary[1] · A. M. Abdullah[1] · M. A. A. Al-dujaili[1]

Received: 1 March 2019 / Revised: 3 August 2019 / Accepted: 8 November 2019

Abstract

This work reports, for the first time, the sintering of the thermally decomposable lead dioxide at a temperature lower than 290 °C. Such low-temperature processing is necessary to avoid the transformation of the conductive lead dioxide to the non-conductive lead oxides via the well-known thermal decomposition processes of lead oxides. Such sintering process provides an important opportunity to find a way toward an efficient and cost-effective alternative for platinum electrodes for the electrochemical applications. It has been found that 90% of the theoretical density can be achieved, for lead dioxide body, via cold sintering process with the help of minor additives of saturated lead nitrate solution and 2 M hydrochloric acid solution. The different characterization analyses could not detect any undesirable phase, while the cyclic voltametery, BET, and the contact angle tests confirmed the suitability of the synthesized body for the electrochemical applications.

Keywords Lead dioxide · PbO_2 · Cold sintering · Electrodes · Platinum · Thermal decomposition

Introduction

Platinum, due to its distinct adsorption properties and ease of fabrication, is the most favorite material to be effectively used as electrode in a wide range of applications. These include the fuel cells, batteries, sensors, and detectors [1–3]. Also, it is an important component in the electrochemical synthesis units of important chemicals including the perchlorates, peroxysulphates, carbohydrates, and ozone. Moreover, it is widely used in studies on the abatement of recalcitrant pollutants by electrochemical methods [4]. However, the enormous demand of industry for platinum and its high cost led to an increasing tendency to find out suitable alternatives for platinum [5].

From the electrochemical point of view, lead dioxide (PbO_2) is the most suitable alternative for platinum [6, 7]. It is a cheap inorganic metal-like oxide showing good stability under high electrical potentials in many environments [8]. The lead dioxide electrodes are usually synthesized by electrodeposition of PbO_2 layer on different conductive substrates; these include titanium, graphite, gold, aluminum, stainless steel, and lead [9–12]. The high cost of titanium, gold, and graphite and the warping and adhesive problems of the PbO_2 layer on aluminum, stainless-steel, and lead are still considerable challenges in the use of the PbO_2-coated electrodes [10, 13, 14].

Sintering, in its various types, is the major manufacturing process for ceramics. However, it could not be used to synthesize a dense body of PbO_2 ceramics. This is because of the decomposition of PbO_2, at low temperature of 290 °C, to a non-conductive phase of lead oxide ($Pb_{12}O_{19}$). Because of this engineering challenge, PbO_2 is considered yet as an unsinterable ceramic [15, 16].

Cold sintering process (CSP) is a new sintering technique which has been recently developed to fabricate ceramics at low temperatures [17]. The "cold sintering" term was coined by Gutmans and Rabinkin for sintering many metals using high pressure and low temperature utilizing the dislocation motion [18]. Jantunen and her colleagues used the CSP to fabricate $LiMoO_4$ ceramics without using the "cold sintering" term to describe their process [19]. Randall and his research group reinvestigated the CSP and used it to fabricate a vast range of ceramics and ceramic composites [17]. They also went a long way to discover the mechanisms of the CSP and to link their experimental findings to the basic phenomena in the field of nucleation and crystallization of the materials.

✉ I. A. D. Al-Hydary
imadali4@uobabylon.edu.iq; imadali4@yahoo.com

[1] Department of Ceramics and Building Materials, College of Materials Engineering, University of Babylon, Hillah, Iraq

Published online: 30 November 2019

They provided that CSP is a dynamic processing technique that starts a lot of new possibilities for fabricating a wide range of materials including oxides, nitrides, and carbides especially that with a high sintering temperature, and composites that could be compatibly co-fired regardless the large difference in the suitable fabrication temperature and the thermal expansion coefficient between metals, polymers, and ceramics. Based on that, in the last few years, the CSP has gotten wide attention for the fabrication of ceramics for many applications especially the dielectrics and electronics [20–24]. Yan and his coworker presented a design of caking-inspired cold sintering to form plastic films in 10 s under the pressure exerted with a finger [25].

As per our best knowledge, the use of CSP to sinter the thermally decomposable material was only very recently reported by Randall and his research group [26, 27]. However, sintering of lead dioxide is not reported before using any type of sintering process [28–31].

The present article illustrates a research work regarding the densification of the PbO_2 powder utilizing the cold sintering process. In order to employ an effective CSP, the solid particles of the ceramic powder must be wetted with a liquid phase containing congruently soluble anions and cations to promote the cold sintering process [32]. In the current work, as PbO_2 is water insoluble oxide, HCl solution and saturated aqueous solution of lead nitrate were selected, after many primary experiments, as solvent and cations supplier, respectively.

Methods and procedures

All the chemicals and materials used in the current work were used as received without further purification or modification. A saturated solution of lead nitrates was prepared by dissolving the appropriate amount of lead nitrate ($(Pb(NO_3)_2$, NLT 99.0%, HIMEDIA) in distilled water. A fresh 2 M hydrochloric acid solution was prepared by dissolving a given volume of HCl acid (35.4% HCl, NLT 99.9%, CDH) with the suitable volume of distilled water. The PbO_2 powder (PbO_2, NLT 99.9%, BTC) was mixed with the lead nitrate solution and the hydrochloric acid solution using pestle and mortar for 1–2 min. The ratios of the lead dioxide to lead nitrate solution and the hydrochloric acid solution in the mixture were 100 g: 2.4 ml: 1.6 ml, respectively.

A freshly prepared mixture was uniaxially pressed under 500 MPa at room temperature of 25 °C for 5 min, then, while the pressure is hold, the temperature was ramped up to 285 °C with a rate of 9 °C/min and isothermally kept for 90 min. The baked sample was left to cool down to room temperature. The prepared samples have a diameter of 12.77 mm, the same of the stainless steel die, and thickness of ~ 1 mm. Most of the characterization method were performed on the "as-prepared" samples as well as "washed" samples which are, after the sintering, immersed in water for 24 h, washed with water, and dried for 3 h at 105 °C.

TEM (Philips CM120) was used in order to investigate the particle morphology and the particle size of PbO_2 starting powder. The particle size distribution was determined using a laser particle size analyzer (Bettersize 2000); a small amount of the starting PbO_2 powder was added to distilled water and subjected to mixing and sonication in order to prepare the suspension required for the test.

The density of the bulk samples was tested using the mass/dimension ratio and the Archimedes' method by using the distilled water as liquid phase. The phase identification analyses were done using X-ray diffractometer (XRD, SHIMADZU 6000, Japan) at room temperature using Cukα radiation (λ = 1.5406 nm), with scanning speed of 5°/min from 10 to 70° of 2 (Bragg angle) for PbO_2 before and after the CSP with an applied power of 40 kv/30 mA. The test was performed for the as-prepared dense sample as well as the washed sample. The samples were milled, by pestle and mortar, and sieved using a 200 mesh sieve then placed on an aluminum holder to be tested.

FE-SEM (MIRA3-TESCAN) system equipped with energy dispersive X-ray detector was used to investigate the microstructure and elemental distribution of the prepared dense samples. The EDS chemical mapping was performed over a scanned area of 20 × 20 μm of as-prepared and washed sample to investigate the chemical and the phase purity of the prepared samples.

The FTIR study was carried out to characterize the PbO_2 powders, lead nitrates, and the bulk samples. The FTIR spectra of the samples were recorded using Shimadzu 1800 (Japan) to evaluate the molecular structure of the functional group in the prepared samples. The FTIR spectra were recorded in the range of 400–4000 cm^{-1} at room temperature.

Nitrogen adsorption/desorption isotherms were obtained using (QSURF) surface area analyzer apparatus. Before analysis, the samples were degassed at 200 °C under a vacuum inside the apparatus. The isotherms were measured at liquid nitrogen temperature in order to determine the surface area and the pores volume.

The prepared specimens were tested with (TH-717) digital micro-Vickers hardness tester with load of 9.8 N and holding time of 15 s.

To confirm the hydrophilicity, which is necessary for electrodes, the contact angle measurements were carried out using an automated contact angle instrument (SL200K series, KINO). The sessile drop technique was followed using deionized water at 25 °C. For triplicate samples, 3 μL droplet was automatically dropped on the surface, and the measurement was achieved within 15 s after the positioning of the drop.

The cyclic voltammetry test (CV) was carried out with an (Wuhan CorrTest) instrument at a potential scan range of − 1–0.4 V and rate of 0.001 VS^{-1}. The electrochemical

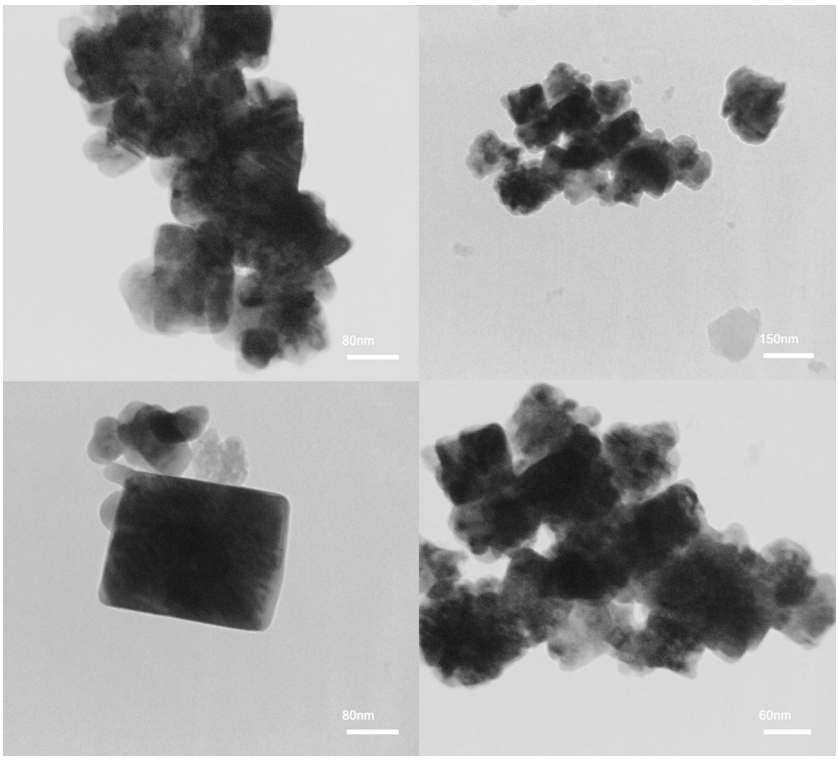

Fig. 1 TEM micrographs of PbO_2 starting powder

performance of two PbO_2 samples was investigated at 25 °C in 2 M KOH solution as an electrolyte. Three electrodes were utilized in this system: a lead dioxide working electrode, a platinum disk auxiliary electrode, and SCE as reference electrode. This test was performed to confirm the electrical conductivity of the prepared dense PbO_2 samples that make them suitable to be used as electrode in the electrochemical processes.

Results and discussion

Figure 1 shows the TEM micrographs of the PbO_2 starting powder which has been used in the current work. It can be noticed that the particles have a wide range of sizes, all below 250 nm, and various shapes including the spherical and polyhedral shapes. Also, the particles are highly aggregated due to their small sizes that produce a high surface energy.

The particle size distribution of the PbO_2 starting powder is shown in Fig. 2, the particle size extends over a wide range from 100 up to 50 μm, and the distribution has a multi-model with D50 of 4.788 μm. These results are in agreement with that obtained from TEM as the laser particle size analyzer measures the primary sizes of the particles as well as their secondary sizes produced due to agglomeration and/or aggregation.

Table 1 shows the trend of the relative density of the green and cold sintered samples compacted at different pressures. As expected, the relative density of the green compacts increases when the applied pressure increases; however, the relative

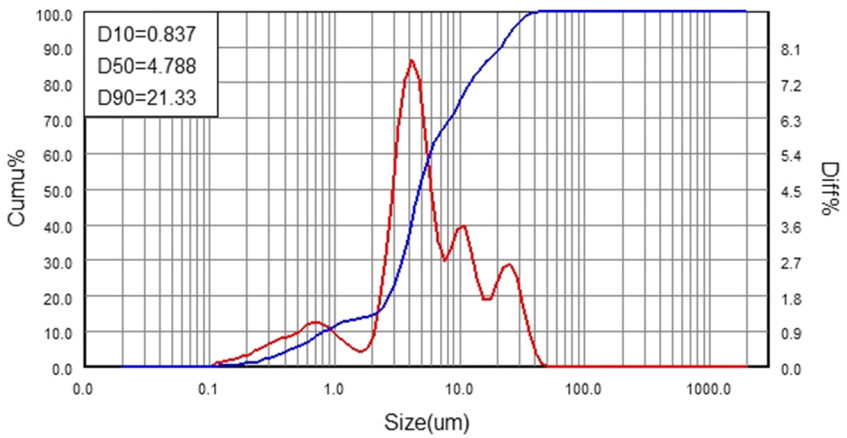

Fig. 2 Particle size distribution of PbO_2 starting powder

Table 1 The trend of the relative density of the green and cold sintered samples of PbO_2 compacted at different pressures

Pressure (MPa)	Green relative density (%)	Relative density (%)
300	70	84.53
400	71	85.28
500	76	90.00

density of the green compacts does not exceed 76% when the applied pressure reaches 500 MPa. If a pressure higher than 500 MPa is used, a cracked green sample is produced. It is clearly seen that each cold sintered sample has a higher relative density as compared with its corresponding green sample. This confirms that a densification has occurred due to the cold sintering process.

The XRD patterns of the PbO_2 starting powder, the as-prepared bulk sample, and the washed bulk sample are given in Fig. 3. The obtained diffraction data for all these samples are in full matching with the ICSD cards (01-073-0851) and (01-072-2440) for α-PbO_2 and β-PbO_2, respectively. Also, an unknown peak with intensity less than 1% could be noticed at 2θ of 44.1° in the pattern of the PbO_2 starting powder.

The Rietveld method for phase quantitative analysis was used to compute the percent of each phase before and after sintering/washing. This method showed that the starting powder is composed of 89.6% α-PbO_2 and 10.4% of β-PbO_2 revealing that α-PbO_2 is the major constituent for the starting powder. This phase was increased up to 98.5% in the bulk as-prepared sample indicating that the cold sintering process stabilizes the α-PbO_2 phase on the expense of the β-PbO_2 phase.

However, washing and drying the sample promote the transformation of α-PbO_2 phase to β-PbO_2 phase as the percent of the α-PbO_2 phase decreases to 92.4%. It is important to note that the unknown peak at 44.1° in the pattern of the starting powder had disappeared after sintering, while a new unknown peak at 37.7° in the pattern of the as-prepared sample was observed. The later unknown peak had also disappeared after washing. The appearance/disappearance of such undefined peaks, in addition to the change in the intensity of the β-PbO_2 peak at 64.3°, confirms that these peaks are related to phase imperfection rather than the presence of another phase. This indicates that the cold sintering process does not cause any detectable thermal decomposition for the lead dioxide.

The EDS chemical mapping of the as-prepared and the washed samples is shown in Fig. 4 and Fig. 5, respectively. This analysis showed that Pb and O, which are homogenously distributed over the scanned area, are the main constituents in both samples, and the Na and N impurities are also presence with low percentage. Two peaks at 6.40 keV and 7.06 keV were also observed in the as-prepared sample corresponding to K_α and K_β spectrum of Fe which contaminated the sample from the steel die due to the use of the HCl acid.

It can be noticed that N impurity in the washed sample is presented with nearly the same percentage of the N in the as-prepared sample; this indicates that N is not belonging to the $Pb(NO_3)_2$ as the lead nitrates are soluble in water. Based on that and in addition to the XRD results, it is believed that the lead nitrates were totally decomposed to PbO_2 during the sintering process.

Figure 6a shows the FTIR spectra of the PbO_2 powder; the high intensity bands located in the range 400–500 cm^{-1} are

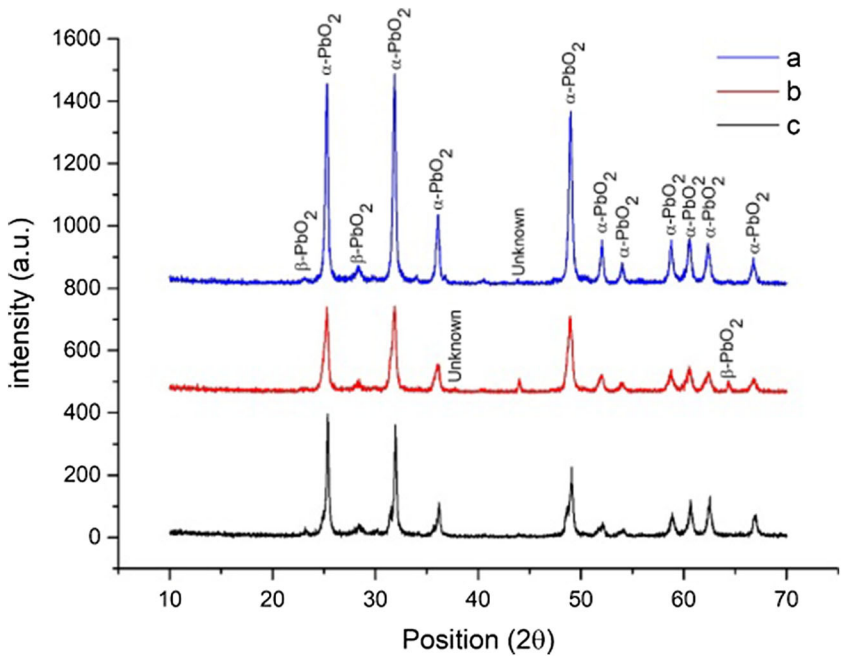

Fig. 3 XRD patterns of (a) PbO_2starting powder, (b) as-prepared bulk sample, and (c) washed bulk sample

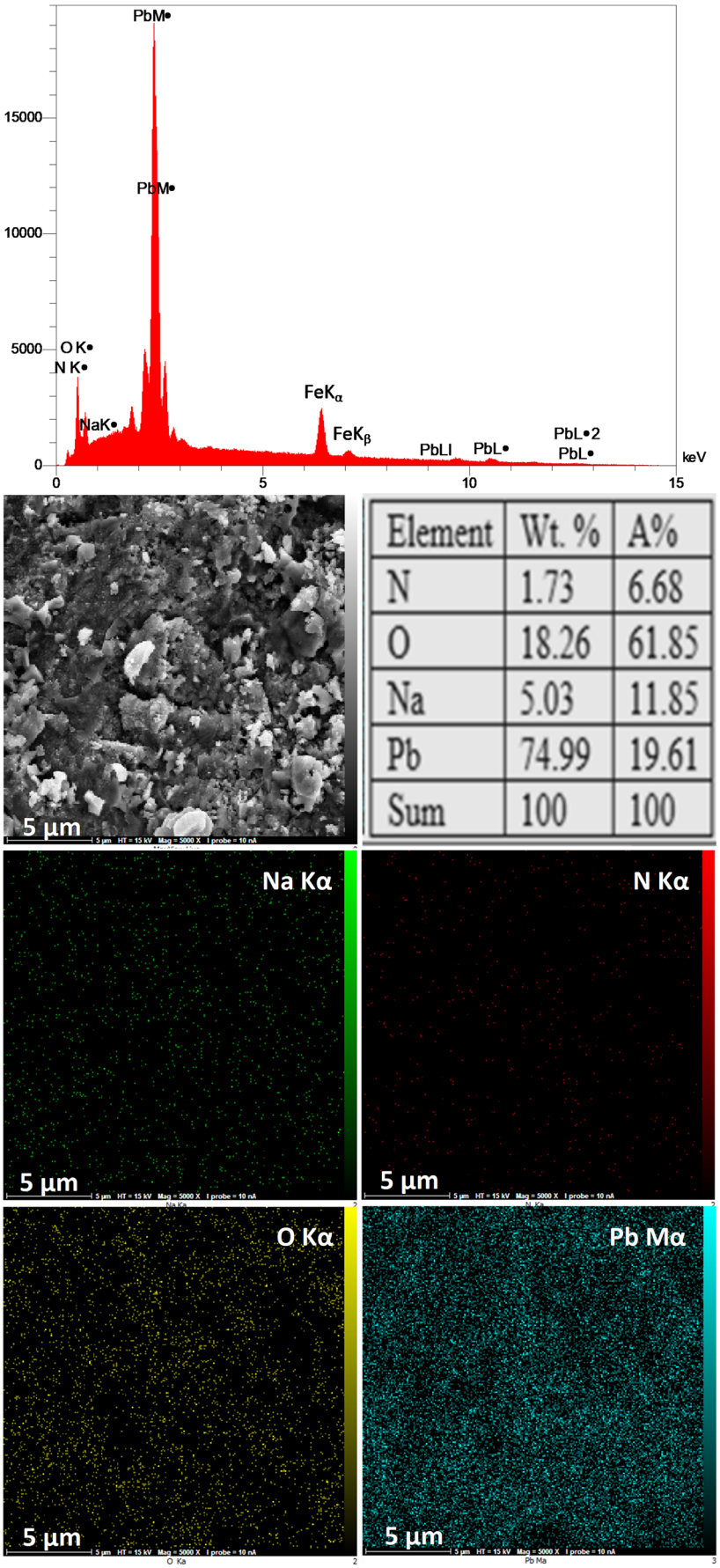

Fig. 4 The EDS chemical analysis and mapping of the unwashed sample

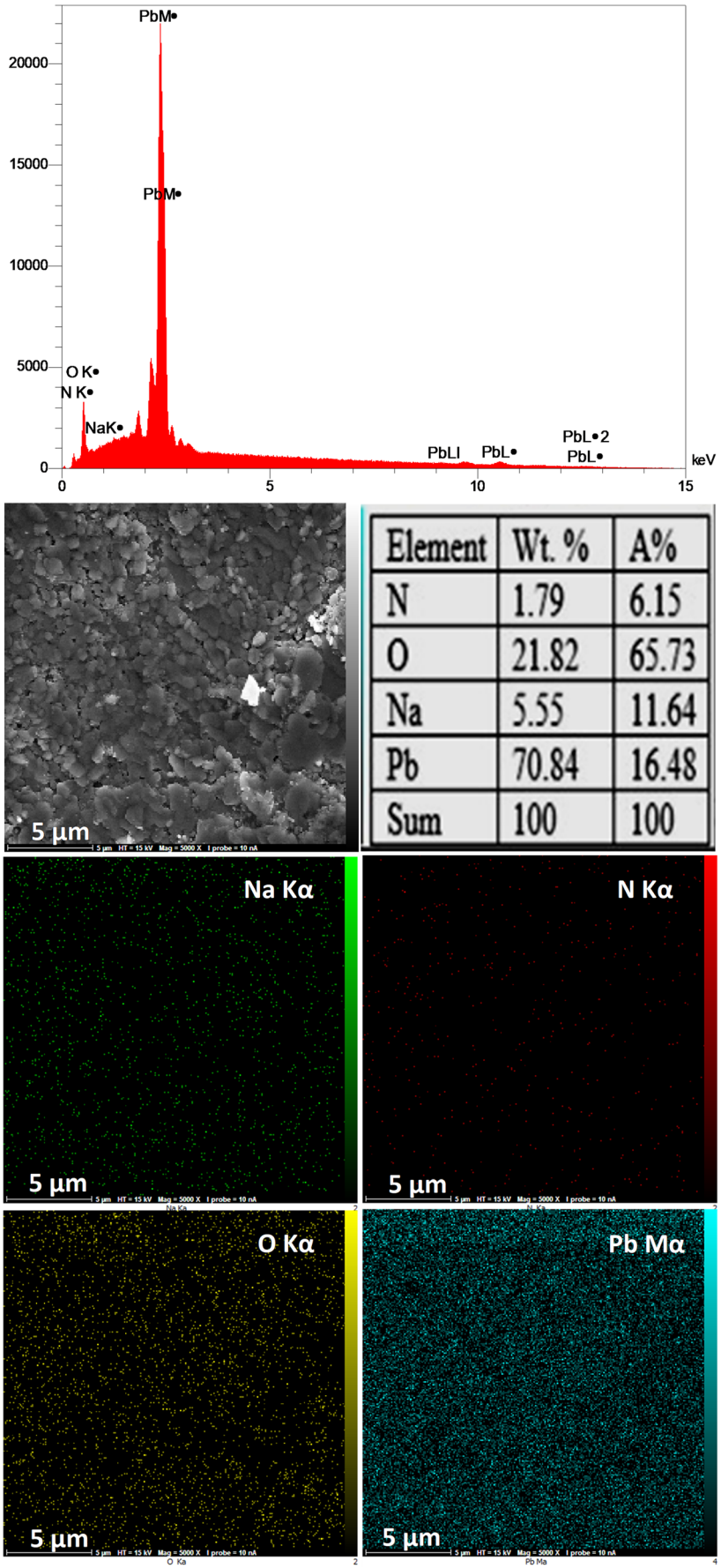

Fig. 5 The EDS chemical analysis and mapping of the water-immersed and washed sample

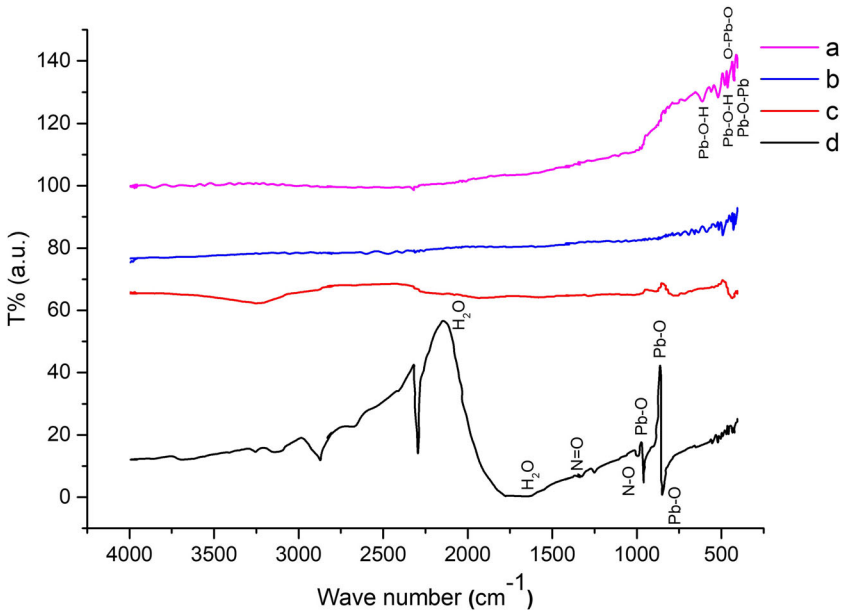

Fig. 6 FTIR spectra of (a) PbO2 starting powder, (b) as-prepared bulk sample, (c) washed bulk sample, and (d) lead nitrates

associated with the O-Pb-O and the Pb-O-Pb bonds. The nonstoichiometric nature of PbO_2 induces it to make Pb-O-H bond which is observed at 550 cm^{-1} and 700 cm^{-1}. No further bands was observed indicating, in addition to the XRD results, the high purity of the PbO_2 powder. Hence, the unknown peak observed at the XRD pattern is more likely to be attributed to phase imperfection. The FTIR spectrum of the $Pb(NO_3)_2$ is shown in Fig. 6d; the bands for the NO_3^+ group

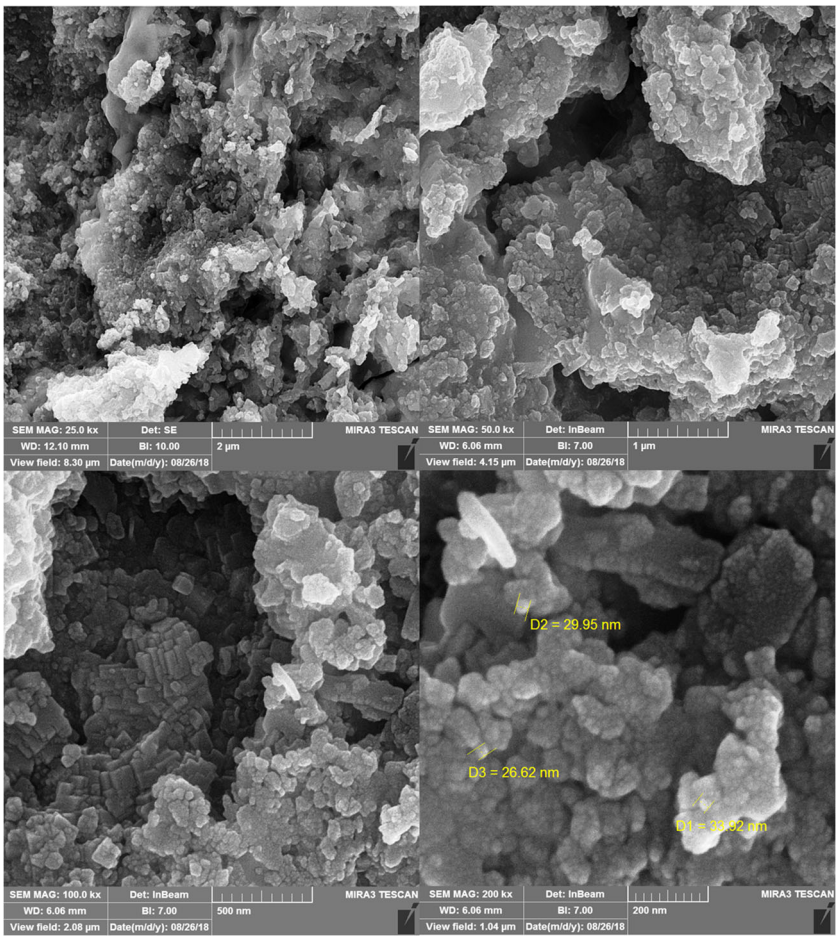

Fig. 7 FE-SEM for the as-prepared PbO_2 bulk sample

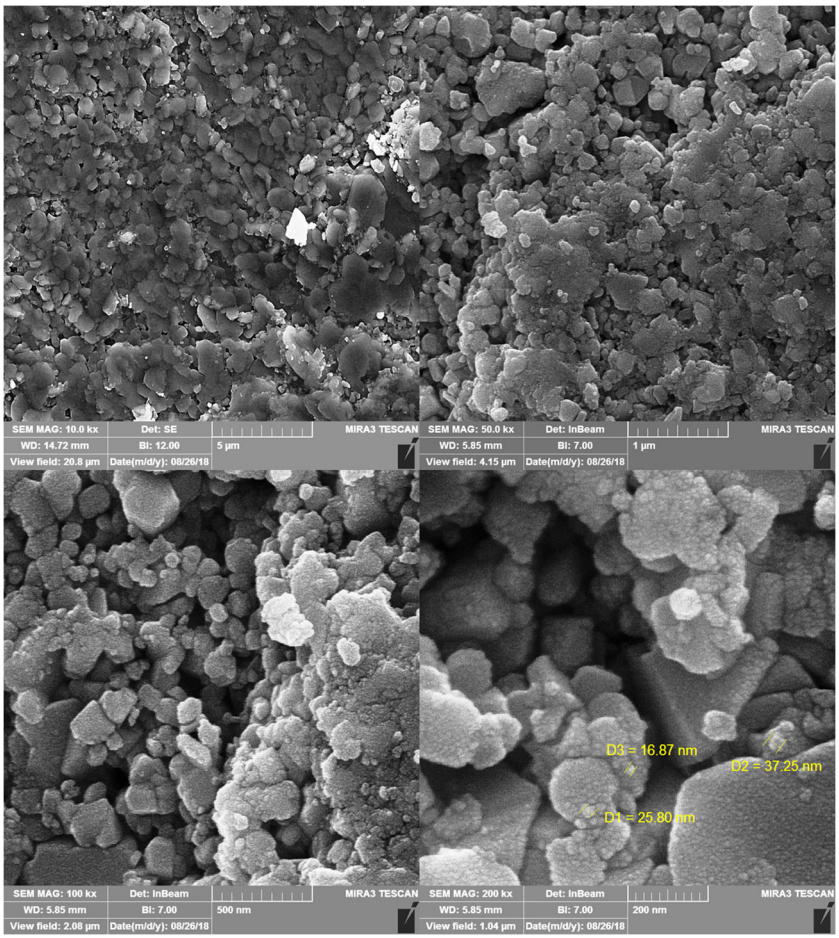

Fig. 8 FE-SEM for the PbO_2 washed bulk sample

were observed at 1406 cm^{-1}. The bands at 1656 cm^{-1} and 2079 cm^{-1} are assigned to H_2O, while the bands at 723, 804, 825, and 1012 cm^{-1} are attributed to Pb-O bonds. The bands at 1072 cm^{-1} and 1768.7 cm^{-1} are owned to N-O and N=O bonds [33–35]. However, no evidence could be noticed regarding the presence of the HCl or $Pb(NO_3)_2$ in the as-prepared as well as the washed samples confirming their thermal decomposition during the sintering process.

Figures 7 and 8 show the SEM images for the as-prepared and washed bulk samples, respectively, at different magnifications. The surface of these samples was subjected to grinding process using SiC grinding papers with grit of 1500. The structure of the as-prepared and washed samples seems to have the same features confirming the absence of any second phase as suggested by the results of the previous analysis. It can be seen that the microstructure of the bulk sample consists of clusters of particles or aggregates with a wide range of sizes. This suggests, as reported in literature [36, 37], that the sintering process has occurred mainly due to the precipitation processes, and the grain growth, if any, is limited under these experimental conditions. During the precipitation process, the system builds a bridge-like between the particles of the primary powder and tries to fill the pore between them. The wide size distribution of the precipitates indicates that the nucleation of the precipitates is a continuous process. The precipitates have different shapes including the polyhedron shape, especially near to the pores, which is not the favorable for the sintering via the dissolution–precipitation process [30].

It can be seen that the pores have a different irregular shapes. This is because the pores in the green body do not have identical shapes and are not fully filled with the liquid phases. Also, the different rates of evaporation of the liquids affect the pores formation as well as their size and shape. Also, the presence of the steps-like crystals in the microstructure of these samples confirms that the sintering process was performed via the dissolution–precipitation process as described by the classical model of Terrace-Ledge-Kink (TLK) to crystal growing on the raw powder particles [21, 38, 39].

Table 2 The microhardness of different PbO_2 bulk samples

Relative density	Microhardness (GPa)
80	1.042
84	1.595
88	1.083
85	1.503

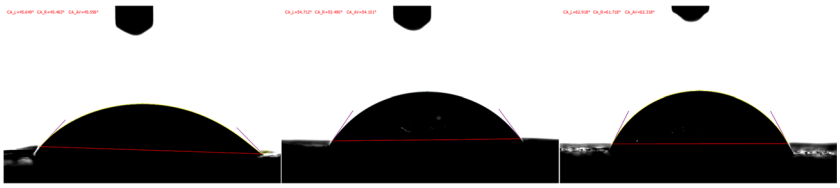

Fig. 9 Contact angle for different PbO_2samples

The BET test revealed that the surface area for the prepared PbO_2 bulk sample was about 9 m^2/g. This surface area is large enough to give a large area of contact between the prepared PbO_2 bulk sample and the electrolyte in the electrochemical applications.

The BET test also showed that the pore volume is around 0.03 cm^3/g. While the mesoporous pore size is around 10.2 nm according to the IUPAC classification. This result confirms the densification effect of the cold sintering process.

The hardness test was performed for four bulk samples with different densities. The results of this test are given in Table 2. All the tested samples have a high microhardness above 1 GPa. The variation in the values of the microhardness may belong to the role of the porosity on the results of the hardness test.

The contact angle between the prepared PbO_2 bulk samples and the distilled water was measured for different samples. As shown in Fig. 9, the values of the contact angle were varied between 45 and 65°; these values indicate the hydrophilicity nature of the prepared PbO_2 which is a very essential requirement for the electrodes in the aqueous base electrolytes.

Figure 10 shows the hysteresis circles for two different PbO_2 bulk samples. In the negative voltametric scan, the samples exhibited comparable anodic peaks at − 0.33 V and − 0.29 V related to an oxidation reaction. In the positive scan, a reduction process occurred at higher cathodic peaks of potential of − 0.76 V and − 0.69 V for both samples.

The differences between the anodic and the cathodic peak values, for both samples, indicate the semi-reversible nature of the electrochemical process. It can be noticed that the current density in both hysteresis circles is greater for the reduction process as compared with the oxidation process; this may have attributed the non-stoichiometric nature of the surface of the PbO_2 samples. In such structure, some Pb ions, which did not exist in the form of highest valance state (+ 4) in the lattice, could be further oxidized by the adsorbed hydroxyl radicals produced by water discharge. The physically adsorbed oxygen is transferred to chemically adsorbed oxygen in this process [40–42]. Anyway, these results confirm that the prepared PbO_2 bulk samples are metal-like conductive and, hence, are suitable for the electrochemical applications.

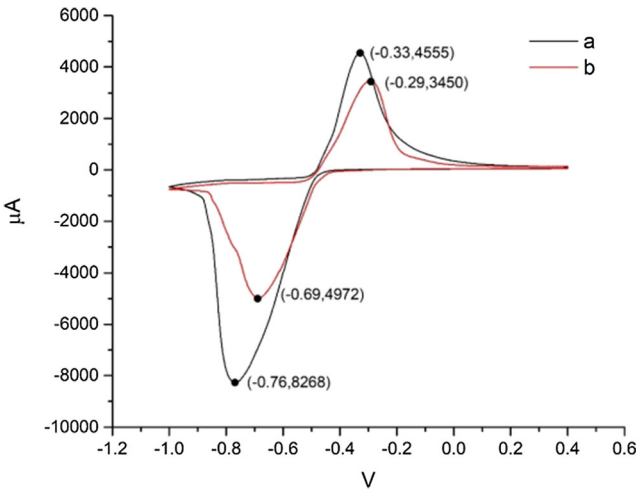

Fig. 10 Cyclic voltammetry curves of two PbO_2 bulk samples

Conclusion

In summary, the newly developed CSP route was utilized to achieve dense ceramic body of the thermally decomposable PbO_2 powder. A low temperature processing was used with the help of both incongruent and congruent dissolution issues. It has been found that low temperature, suitable high pressure, and just baking time were enough to sinter PbO_2 powder, without a transformation to the nonconductive phases, to a density reaching up to 90% of theoretical density. The purity of the material was guaranteed during the process, and no second phase was noticed. Hydrophilicity, high surface area, and the most important electrochemical conductivity were confirmed for the densified samples.

References

1. Wilke, D., Müller, H., Kolytsheva, N.: Activated platinum electrodes as transducer for a glucose sensor using glucose oxidase in a photopolymer membrane. Fresenius. J. Anal. Chem. **357**, 534–538 (1997)
2. Oswin, B.H.G., Phi, D.: Platinum metals in the fuel cell. **8**, 42–48 (1964).
3. Johnson, D.C., LaCourse, W.R.: Liquid chromatography with pulsed electrochemical detection at gold and platinum electrodes. Anal. Chem. **62**, 589A–597A (1990)
4. Amadelli, R., Velichenko, A.B.: Lead dioxide electrodes for high potential anodic processes. J. Serbian Chem. Soc. **66**, 834–845 (2001)
5. Hou, Y., Wang, D., Yang, X.H., Fang, W.Q., Zhang, B., Wang, H.F., Lu, G.Z., Hu, P., Zhao, H.J., Yang, H.G.: Rational screening low-cost counter for dye-sensitized solar cells. Nat. Commun. **4**, (2013)

6. Morris, J.M., Jin, S., Wang, J.Q., Zhu, C.Z., Urynowicz, M.A.: Lead dioxide as an alternative catalyst to platinum in microbial fuel cells. Electrochem. Commun. **9**, 1730–1734 (2007)
7. Cordeiro, J.M.M., de Azevedo, D.H.M., Barretto, T.C.M., Sambrano, J.R.: Conducting behavior of crystalline a-PbO_2 as revealed by DFT calculations. Mater. Res. **21**, 1–7 (2018)
8. Payne, D.J., Egdell, R.G., Hao, W., Foord, J.S., Walsh, A., Watson, G.W.: Why is lead dioxide metallic? Chem. Phys. Lett. **411**, 181–185 (2005)
9. Jones, P., Lind, R., Wynne-Jones, W.F.K.: The behaviour of the lead dioxide electrode. Trans. Faraday Soc. **55**, 972–979 (1954)
10. Mohd, Y., Pletcher, D.: The fabrication of lead dioxide layers on a titanium substrate. Electrochim. Acta. **52**, 786–793 (2006)
11. Wang, H., Dai, D., Zhang, X., Wu, X.D.: Preparation and characterization of PbO_2 on aluminum substrate. Mater. Sci. Forum. **610–613**, 288–292 (2009)
12. Song, Y., Wei, G., Xiong, R.: Structure and properties of PbO_2-CeO_2 anodes on stainless steel. Electrochim. Acta. **52**, 7022–7027 (2007)
13. Yao, Y., Zhao, C., Zhu, J.: Preparation and characterization of PbO_2-ZrO_2 nanocomposite electrodes. Electrochim. Acta. **69**, 146–151 (2012)
14. Dan, Y., Lin, H., Chen, L., Zhang, L., Su, J., Yue, H., Cai, X.: A composite electrodeposited PbO2/SnO2positive electrode material for hybrid supercapacitors. RSC Adv. **5**, 98983–98989 (2015)
15. Guilder, S.M., Simon, A.C.: Thermal decomposition mechanism of formed and cycled lead dioxide electrodes and its relationship to capacity loss and battery failure. J. Electrochem. Soc. **121**, 1546–1551 (1974)
16. Gavrichev, K., Bolshakov, A., Kondakov, D., Khoroshilov, A., Denisov, S.: Thermal transformations of lead oxides. J. Therm. Anal. Calorim. **92**, 857–863 (2008)
17. Guo, H., Baker, A., Guo, J., Randall, C.A.: Cold sintering process: a novel technique for low-temperature ceramic processing of ferroelectrics. J. Am. Ceram. Soc. **99**, 3489–3507 (2016)
18. Gutmanas, E.Y., Rabinkin, A., Roitberg, M.: Cold sintering under high pressure. Scr. Metall. **13**, 11–15 (1979)
19. Kähäri, H., Teirikangas, M., Juuti, J., Jantunen, H.: Dielectric properties of lithium molybdate ceramic fabricated at room temperature. J. Am. Ceram. Soc. **97**, 3378–3379 (2014)
20. Guo, H., Guo, J., Baker, A., Randall, C.A.: Cold sintering process for ZrO_2-based ceramics: significantly enhanced densification evolution in yttria-doped ZrO_2. J. Am. Ceram. Soc. **100**, 491–495 (2017)
21. Boston, R., Guo, J., Funahashi, S., Baker, A.L., Reaney, I.M., Randall, C.A.: Reactive intermediate phase cold sintering in strontium titanate. RSC Adv. **8**, 20372–20378 (2018)
22. Guo, J., Pfeiffenberger, N., Beese, A., Rhoades, A.M., Gao, L., Baker, A., Wang, K., Bolvari, A., Randall, C.A.: Cold sintering $Na_2Mo_2O_7$ ceramic with polyetherimide (PEI) polymer to realize high performance composites and integrated multilayer circuits. ACS Appl. Nano Mater. **8**, 3837–3844 (2018)
23. Funahashi, S., Guo, J., Guo, H., Wang, K., Baker, A.L., Shiratsuyu, K., Randall, C.A.: Demonstration of the cold sintering process study for the densification and grain growth of ZnO ceramics. J. Am. Ceram. Soc. **100**, 546–553 (2017)
24. Heidary, D.S.B., Guo, J., Seo, J.-H., Guo, H., Rajagopalan, R., Randall, C.A.: Microstructures and electrical properties of V_2O_5 and carbon-nanofiber composites fabricated by cold sintering process. Jpn. J. Appl. Phys. **57**, 025702 (2018)
25. Xie, M., Che, Y., Liu, K., Jiang, L., Xu, L., Xue, R., Drechsler, M., Huang, J., Tang, B.Z., Yan, Y.: Caking-inspired cold sintering of plastic supramolecular films as multifunctional platforms. Adv. Funct. Mater. **28**, 1–8 (2018)
26. Bang, S.H., De Beauvoir, T.H., Randall, C.A.: Densification of thermodynamically unstable tin monoxide using cold sintering process. J. Eur. Ceram. Soc. **39**, 1230–1236 (2018)
27. Nakaya, H., Iwasaki, M., Herisson, T., Beauvoir, D., Randall, C.A.: Journal of the European Ceramic. Society Applying cold sintering process to a proton electrolyte material : CsH_2PO_4. J. Eur. Ceram. Soc. 0–1 (2018)
28. Baker, A., Guo, H., Guo, J., Randall, C., Green, D.J.: Utilizing the cold sintering process for flexible–printable electroceramic device fabrication. J. Am. Ceram. Soc. **99**, 3202–3204 (2016)
29. Guo, J., Berbano, S.S., Guo, H., Baker, A.L., Lanagan, M.T., Randall, C.A.: Cold sintering process of composites: bridging the processing temperature gap of ceramic and polymer materials. Adv. Funct. Mater. **26**, 7115–7121 (2016)
30. Guo, H., Guo, J., Baker, A., Randall, C.A.: Hydrothermal-Assisted Cold Sintering Process: A new guidance for low-temperature ceramic sintering. ACS Appl. Mater. Interfaces. **8**, 20909–20915 (2016)
31. Guo, H., Baker, A., Guo, J., Randall, C.A.: Protocol for ultralow-temperature ceramic sintering: an integration of nanotechnology and the cold sintering process. ACS Nano. **10**, 10606–10614 (2016)
32. Maria, J.P., Kang, X., Floyd, R.D., Dickey, E.C., Guo, H., Guo, J., Baker, A., Funihashi, S., Randall, C.A.: Cold sintering: current status and prospects. J. Mater. Res. **32**, 3205–3218 (2017)
33. Silverstein, R.M., Webster, F.X., Kiemle, D.J.: Silverstein - spectrometric identification of organic compounds 7th ed.pdf. JHON WILEY & SONS, INC., New York (2005).
34. Nyquist, R.A., Kagel, R.O.: Infrared spectra of inorganic compounds. Acadimic Press, New York and London (1971)
35. Macavei, S., Rada, M., Zagrai, M., Rada, S., Balan, R., Erhan, R., Macavei, S., Rada, M., Zagrai, M., Rada, S.: Spectroscopic characterization of a lead – lead dioxide automobile battery. Anal. Lett. **0**, 1–11 (2018)
36. Guo, J., Baker, A.L., Guo, H., Lanagan, M., Randall, C.A.: Cold sintering process: a new era for ceramic packaging and microwave device development. J. Am. Ceram. Soc. **100**, 669–677 (2017)
37. Bouville, F., Studart, A.R.: Geologically-inspired strong bulk ceramics made with water at room temperature. Nat. Commun. **8**, (2017)
38. Sohrabi Baba Heidary, D., Lanagan, M., Randall, C.A.: Contrasting energy efficiency in various ceramic sintering processes. J. Eur. Ceram. Soc. **38**, 1018–1029 (2018)
39. Guo, J., Guo, H., Baker, A.L., Lanagan, M.T., Kupp, E.R., Messing, G.L., Randall, C.A.: Cold sintering: a paradigm shift for processing and integration of ceramics. Angew. Chemie - Int. Ed. **55**, 11457–11461 (2016)
40. Zhang, W., Lin, H., Kong, H., Lu, H., Yang, Z., Liu, T.: Preparation and characterization of lead dioxide electrode with three-dimensional porous titanium substrate for electrochemical energy storage. Electrochim. Acta. **139**, 209–216 (2014)
41. Abaci, S., Tamer, U., Pekmez, K., Yildiz, A.: Performance of different crystal structures of PbO_2 on electrochemical degradation of phenol in aqueous solution. Appl. Surf. Sci. **240**, 112–119 (2005)
42. Rada, S., Rus, L., Rada, M., Culea, E., Aldea, N., Stan, S., Suciu, R.C., Bot, A.: Synthesis , structure , optical and electrochemical properties of the lead sulfate-lead dioxide-lead glasses and vitroceramics. Solid State Ionics. **274**, 111–118 (2015)